

Quantitative Evaluation of Several Partial Fourier Reconstruction Algorithms Used in MRI

G. McGibney, M. R. Smith, S. T. Nichols, A. Crawley

Partial Fourier reconstruction algorithms exploit the redundancy in magnetic resonance data sets so that half of the data is calculated during image reconstruction rather than acquired. The conjugate synthesis, Margosian, homodyne detection, Cuppen and POCS algorithms are evaluated using spatial frequency domain analysis to show their characteristics and where limitations may occur. The phase correction used in partial Fourier reconstruction is equivalent to a convolution in the frequency domain and the importance of accurately implementing this convolution is demonstrated. New reconstruction approaches, based on passing the partial data through a phase correcting, finite impulse response (FIR), digital filter are suggested. These FIR and MoFIR algorithms have a speed near that of the Margosian and homodyne detection reconstructions, but with a lower error; close to that of the Cuppen/POCS iterative approaches. Quantitative analysis of the partial Fourier algorithms, tested with three phase estimation techniques, are provided by comparing artificial and clinical data reconstructed using full and partial Fourier techniques.

Key words: partial Fourier; phase correction; FIR filter.

INTRODUCTION

Partial Fourier reconstruction algorithms exploit the redundancy in the magnetic resonance (MR) data set. Such algorithms are useful when asymmetric data sets arise in spin and gradient echo MR imaging. The algorithms discussed here are the conjugate synthesis (1), Margosian *et al.* (2, 3), homodyne detection (4), Cuppen *et al.* (5) and Projection onto Convex Sets (POCS) methods (6, 7). The recent review paper by Liang *et al.* (8) has provided an explanation and qualitative comparison of these algorithms. The alternative spatial frequency domain viewpoint used in this paper indicates both the limitations of the existing methods and a faster approach to implementing POCS. This analysis suggests new reconstruction approaches, based on passing the partial data through a phase correcting, finite impulse response (FIR), digital filter. All the partial Fourier reconstruction algorithms will be evaluated in conjunction with three phase estimation techniques: Margosian's low frequency filtered estimate (2), the generalized series (9) and a 2D polynomial model estimate (10, 11). A quantitative comparison

of the partial Fourier reconstructions with the full Fourier images is obtained using both artificial and real clinical data.

THEORETICAL ANALYSIS OF EXISTING PARTIAL FOURIER ALGORITHMS

Partial Fourier algorithms perform considerable data manipulation in either (or both) the image and spatial frequency (original data) domains. A number of limitations can be exposed by providing a complete analysis of the algorithms in a single domain. This new information can be used to suggest new algorithms or at least new directions to take to overcome deficiencies.

For easy 1D and 2D image comparison, all 2D images, $\rho(x, y)$, will be displayed with the partial data dimension placed horizontally. It is therefore convenient to assume that the original data, $s(u, v)$; $-N/2 \leq v < N/2$ is inverse discrete Fourier transformed (DFT) in the v dimension to give a new data matrix, $s_y(u)$. Each row of $s_y(u)$, non-zero for $-m \leq u < N/2$, must be reconstructed to form the corresponding image row of $\rho(x, y)$, and can be considered as an independent data set.

Conjugate Synthesis, Margosian, and Homodyne Detection Imaging

Conjugate synthesis imaging (1) attempts to reconstruct a full data matrix based on the assumption that the final image $\rho(x, y)$ has only real components (i.e., no phase terms). The procedure uses the complex conjugate of the known data $[0 \leq u < N/2]$ to fill in the unknown data. The image is reconstructed using an inverse DFT on the completed $s_y(u)$ data set.

The Margosian partial Fourier algorithm (2) multiplies the data set, $s_y(u)$, by a merging filter, with a frequency response $H(u)$, to produce a new data set $s'_y(u)$ with its lower and negative frequencies filtered. This filtering smooths the transition between calculated and known data to reduce Gibbs' ringing during the DFT operation which follows. The data are then inverse Fourier transformed to the image space and each pixel multiplied by the phase estimator function, $\theta_y(x) = e^{-i\phi_y(x)}$, where $\phi_y(x)$ is the phase estimate. In the frequency domain, this is equivalent to convolving the filtered data with the Fourier transform (FT) $\Theta_y(u)$ of the phase estimate $\theta_y(x)$ giving

$$s''_y(u) = \{s_y(u)H(u)\} \otimes \Theta_y(u) \text{ where } \Theta_y(u) = FT(\theta_y(x)). \quad [1]$$

The reconstructed image is taken to be the twice the real part of the image. This is equivalent to adding the frequency domain data to the reflected conjugate of itself.

MRM 30:51-59 (1993)

From the Department of Electrical and Computer Engineering, and the Department of Radiology (A.C.), University of Calgary, Calgary, Alberta, Canada.

Address correspondence to: M. R. Smith, Ph.D., Department of Electrical and Computer Engineering, University of Calgary, 2500 University Drive, N.W., Calgary, Alberta, Canada T2N 1N4.

Received May 4, 1992; revised October 27, 1992; accepted January 26, 1993.

0740-3194/93 \$3.00

Copyright © 1993 by Williams & Wilkins

All rights of reproduction in any form reserved.

The frequency domain analysis of the Margosian method is shown in Fig. 1.

The Margosian image is normally displayed using a magnitude display. One of the problems with the magnitude display of images is the noise bias which leads to a decreased detectability for low intensity objects. This can be avoided by displaying a phase corrected real image (12–14) provided that the phase estimator is not correlated to the noise (10). Since the images obtained from a partial Fourier reconstruction are commonly displayed using a magnitude display, it is not often realized that these images are phase corrected if properly reconstructed. If these images were displayed as a real data set, then the improved low intensity detectability suggested by Berstein *et al.* (13) would become available. This is the essence of the homodyne detection approach (4) which is equivalent to a Margosian reconstruction with a real rather than a magnitude display of the reconstructed image.

Cuppen and POCS Methods

These iterative approaches attempt to overcome the shortcomings of the Margosian method. The Lindskog Cuppen implementation (15) inverse Fourier transforms the original data to the image domain where it is conjugated and multiplied by $e^{j2\phi_y(x)}$. This new image is then Fourier transformed back into the spatial frequency domain to be used to fill in the missing data points. The process is then iterated until a suitable convergence is found.

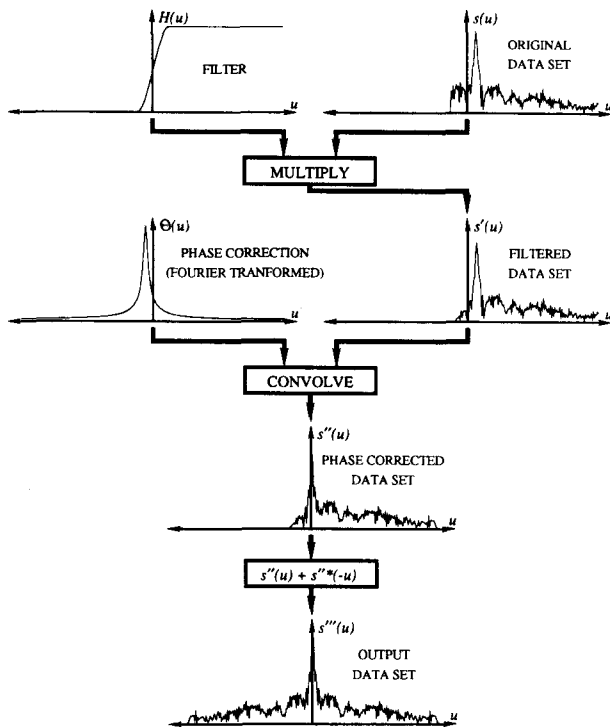


FIG. 1. Frequency domain analysis of the Margosian/homodyne detection partial Fourier reconstruction method. Removal of the phase correction stage provides the analysis for the conjugate synthesis approach.

The frequency domain analysis of this Cuppen implementation is shown in Fig. 2. Conjugating the data in the image domain is equivalent to conjugating and reflecting the spatial frequency domain data around the zero frequency point. This also reverses the sign of the phase error in the image domain, which must be corrected by multiplying with the function $\theta'_y(x) = e^{j2\phi_y(x)}$. The image phase correction operation corresponds to a convolution in the frequency domain with the Fourier transform of $\theta'_y(x)$. Finally the new data set is placed in the original data set locations where no data had been collected, and the process iterated.

POCS (6, 7) is based on the principle that the correct image is the intersection of all images whose Fourier transform agrees with the measured partial data and all images whose phase is the same as the phase estimate. To find the intersection of these two images sets, the data set is first inverse Fourier transformed into the image domain, where the complex values of the image are projected onto a line that is at an angle equal to the phase estimate,

$$\rho_{y,corrected}(x) = |\rho_y(x)| \cos[\hat{\phi}_y(x) - \phi_y(x)] e^{j\phi_y(x)}. \quad [2]$$

The new image is then Fourier transformed back to the spatial frequency domain where it is used to replace the unknown data. The process is repeated and on the last iteration, instead of substituting the new data into the data set from the previous iteration, a merging filter is used.

The relationship between the POCS and Cuppen's algorithms is more obvious if the projection operation is

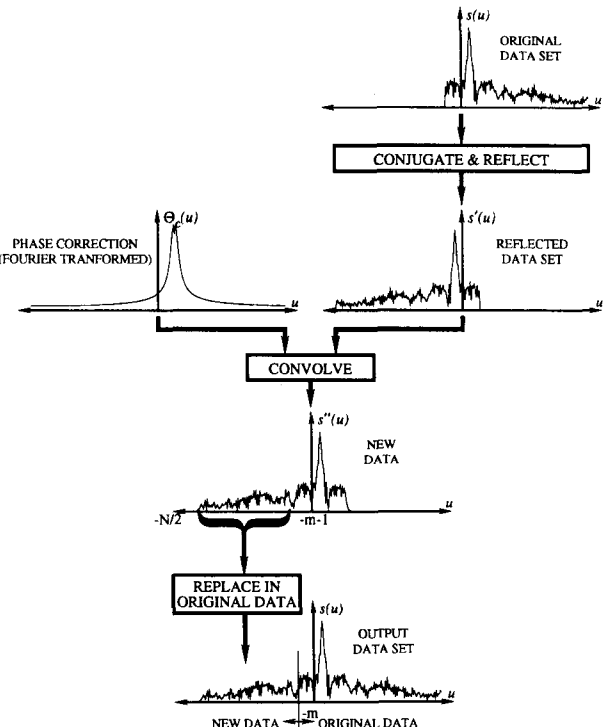


FIG. 2. Frequency domain analysis of the Cuppen's partial Fourier reconstruction algorithm. The POCS algorithm is equivalent to averaging the Cuppen's corrected data with the original data until the final iteration, when a merging filter is applied.

reworked (10)

$$\rho_{y,\text{corrected}}(x) = [\rho_y^*(x)e^{j2\hat{\phi}_y(x)} + \rho_y(x)]/2. \quad [3]$$

This simpler form contains constant trigonometric terms that need only be calculated on the first iteration, and no magnitude operations, so that it executes twice as fast as the original POCS algorithm. The first term of the reworked equation is equivalent to Cuppen’s algorithm. The POCS projection operation then averages this “Cuppen” output with the original data, limiting the change in the new estimate and the convergence, but improving the overall stability. The merging operation between the original and derived data that occurs on the last step reduces the Gibbs’ ringing in the image associated with the discontinuity in the frequency domain.

FIR AND MOFIR RECONSTRUCTIONS

One reason that partial Fourier reconstruction algorithms are not as successful in practice as in theory is associated with distortions introduced during the phase correction. Multiplying an image with a phase correction $\theta_y(x)$ in the spatial domain is equivalent to circularly convolving the spatial frequency domain $s_y(u)$ with $\Theta(u) = FT[\theta_y(x)]$. Figure 3 schematically illustrates this operation. Many of the points in $s_y(u)$ are invalid since they were not collected. The phase correcting convolution smears these invalid points into the legitimate data, decreasing the size of the valid data. The problem is greater for large data asymmetries since the data, $s_{y,\text{actual}}(u); u \approx -m$, will then have a large amplitude. The application of the merging filter, typically a shifted Hanning filter, in the Margosian partial Fourier method would further decrease the size of the valid data. In addition, the phase correction operation distorts the characteristics of the filter so that its merging action is less than ideal.

The first pass through the Cuppen algorithm has the same distortion problems with the convolution operator as does the Margosian incomplete data set with its zeros in the range $u < -m$. Each successive iteration however produces a better estimate of these values and typically

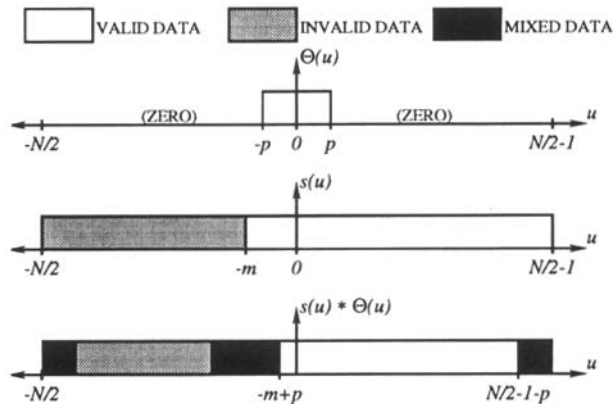


FIG. 3. Phase correction in the image domain corresponds to a circular convolution operation in the frequency domain. Edge effect data distortions will occur because of the incomplete data set. The distortions are reduced by having a low bandwidth phase estimator.

three or four iterations are sufficient to reconstruct the image (5). A further complication occurs after the first iteration with the Cuppens and POCS algorithms as the circular convolution mixes (distorts) the high (valid) positive and negative frequency components responsible for high resolution image characteristics. The importance of this effect (not shown in Fig. 2) depends on the amplitude of the high frequency components.

The degree of distortion introduced by the phase correction is directly related to how (and when) the merging filter is applied, the bandwidth of the phase correction operation, $\Theta_y(u)$, and whether the phase correction is applied by multiplication in the spatial domain (circular convolution) or by direct convolution in the frequency domain where the edge effects of the convolution can possibly be more easily controlled. This direct convolution is equivalent to passing the partial data through a finite impulse response filter (FIR) digital filter.

Preliminary work by McGibney *et al.* (10) has shown that it is possible to directly obtain a narrow bandwidth 2D polynomial phase estimate (11) for spin-echo images. For gradient-echo images, a narrow bandwidth phase estimator could be obtained using a windowed version of the phase estimator,

$$\Theta_{\text{windowed}}(u) = \Theta(u)W(u); W(u) = 1; |u| \leq p \quad [4]$$

$$= 0; |u| > p$$

where $2p + 1$ is the window length (bandwidth) of the phase estimator. The data set is then passed through (convolved with) this FIR filter to phase correct the positive data frequencies. The short filter length implies that direct convolution would be computationally efficient (Order(2pN) complex operations). The negative frequencies can be determined simply by applying conjugate symmetry to the phase corrected data.

However, this simplistic approach would lead to problems if the phase was not completely corrected as the associated discontinuity would create low frequency ringing in the image as with the other algorithms. Instead a merging filter (e.g., a shifted Hanning filter) is applied to the phase corrected data before it is reflected and added to itself. The merging filter’s transition should be kept narrow enough to ensure that little of the distorted edges of the phase corrected data is introduced into the image. (There is a trade off between the need to ensure smooth data merging and the requirement to reject data distorted during the phase correction. It may be possible for the merging filter to have a narrower transition that used in the Margosian filtering since the phase correction has already occurred.) The data is then added to the time reversed conjugate of itself to produce a full Fourier data set which can be transformed to produce an image. The frequency domain analysis of the FIR partial Fourier algorithm is shown schematically in Fig. 4.

A closer look at the spatial frequency domain expression of the Margosian (Fig. 1) and FIR approaches (Fig. 4) shows that the only difference in the algorithms is the order of phase correction and filtering. This difference is significant since these operators do not commute, despite

statements to the contrary by Nolls *et al.* (4). The difference between the two methods becomes greater as the phase shifts become larger.

The merging filter using in the Margosian and homodyne techniques was designed to smooth the transition between known and zero values to avoid Gibbs' ringing during reconstruction. The merging filter in the *FIR* algorithm also smooths the transition, but is designed more to remove the data distorted by the phase correction edge effects. The differences are schematically demonstrated

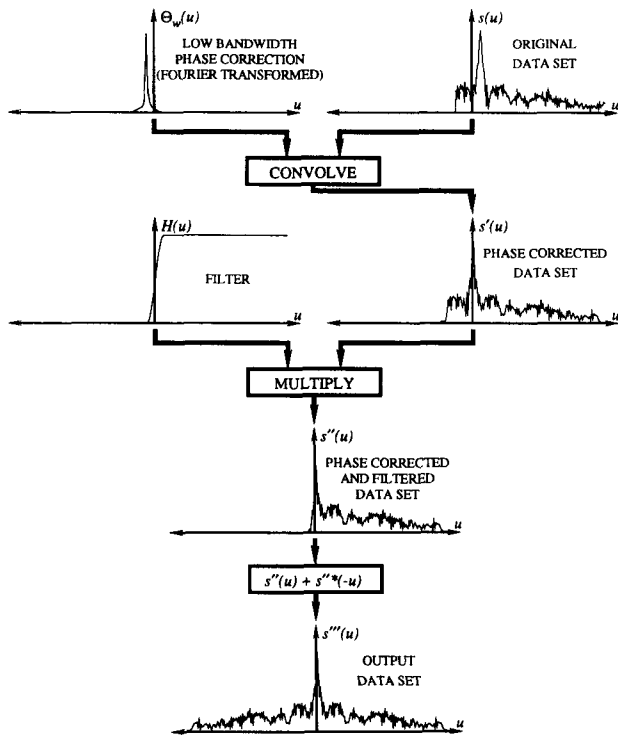
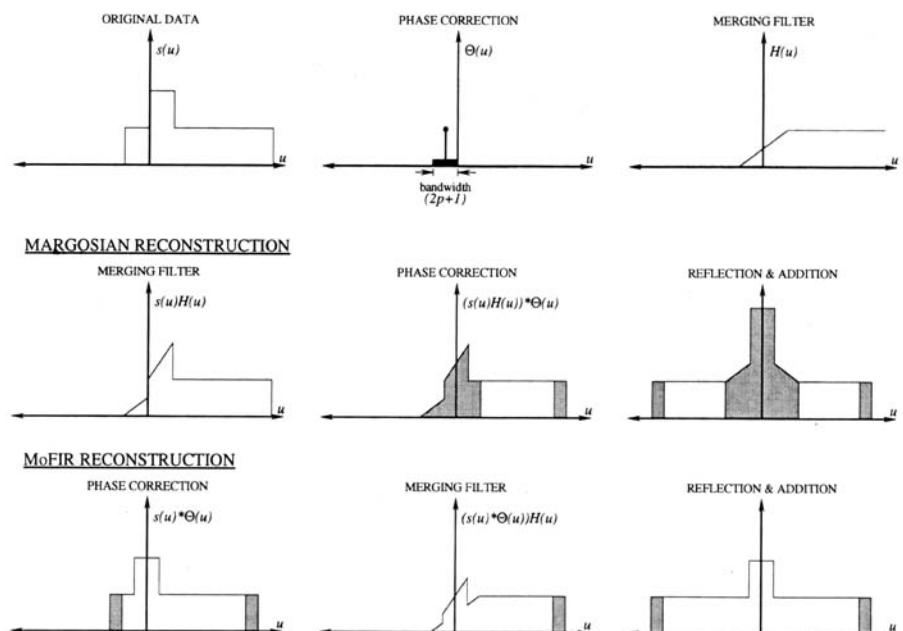


FIG. 4. Frequency domain analysis of the *FIR* and *MoFIR* partial Fourier reconstruction algorithms.

in Fig. 5 which represents some simplistic data that is shifted in the frequency domain by the effect of a simple linear phase term. The phase correction operation is represented by $\Theta(u) = \delta(u - n)$. The merging filter is illustrated using a ramp filter although a shifted Hanning filter would actually be used. The shaded areas in Fig. 5 schematically show the edge distortions that would be present if the phase correction operator had a bandwidth of $2p + 1$. It can clearly be seen that the amount of data affected by the convolution edge effects is considerably lower in the *FIR* approach. The Cuppen/POCS algorithms achieve a similar reduction in edge effects by virtue of their iteration. The reason that the homodyne detection and Margosian reconstructions are limited to images with slowly varying phase (small p) can be seen by the large shaded area for these algorithms. The use of a merging filter prior to the phase correction means that the errors are introduced directly into the large amplitude terms around $|u| \approx 0$, maximizing the distortion.

As will be seen in the reconstructed images, the simplistic approach of the *FIR* reconstruction is degraded by the windowing operation on the phase estimates which introduces truncation artifacts if the true bandwidth is high. This is a problem for gradient echo images where a really narrow bandwidth phase estimator has not yet been found (10). These artifacts are reduced in the modified *FIR* (*MoFIR*) approach which uses all the phase correction function, $\Theta(u)$, without truncating it. This however reintroduces some of the convolution edge effects discussed earlier. However if the phase estimator is properly chosen, its values outside the range $\pm p$ are still small so that the smearing of the noncollected data will not extend too far into the valid data and will be effectively removed by the use of the narrow transition merging filter. When successful at reconstruction, this algorithm phase corrects the data so that the image can be displayed with a real display to obtain increased low

FIG. 5. Schematic diagram showing the distortions introduced into the Margosian/homodyne partial Fourier reconstructed data set as the merging filter is applied prior to the phase correction. The *FIR* algorithm removes this distortion and accounts more accurately for the edge effects (shaded areas) associated with the phase correction operator's bandwidth.



intensity detectability mentioned for the homodyne technique.

The *MoFIR* phase correction convolution can be implemented directly in the frequency domain. However, the long length of the phase estimator means that it is more computationally efficient ($Order(N \log_2 N)$ compared to $Order(2pN)$ complex operations) to inverse Fourier transform the partial data into the image domain, multiply by the phase correction, Fourier transform back to the frequency domain to apply the merging filter before reflecting the data and reconstructing. Thus the *MoFIR* reconstruction is “2 FFTs” slower than the Margosian approach, but computationally more efficient than the Cuppens and POCS approaches which are more than “2l FFTs” slower, where l is the number of iterations.

TEST METHODS AND RESULTS

Two test images were evaluated. The first was an artificial image, a simple box shape (see Fig. 6A) generated in the spatial frequency domain from a truncated sinc function. This artificial image was modified with a quadratic global phase error and two rapid localized phase changes (0.1π and 0.5π high, 5 pixels wide, respectively). These phase errors represent static field and instrumentation effects and a small and large flow induced phase changes. Both exact and inaccurate (quadratic only) phase estimates were supplied to the partial Fourier algorithms. This was intended to correspond to practical situations where the exact phase is not determined because of the effect of image noise or the nature of the phase estimation algorithm.

Analysis on artificially generated data can be rightly criticized as being unrealistic and not representing the true clinical picture. However, when artificially generated data is used in conjunction with clinical data, it can give an insight on the reasons why certain distortions appear on the clinical data. The final test was on a high signal-to-noise clinical image: an axial view of the head acquired with a spin echo series and a data set size of 256×256 (Fig. 6B). The phase of the image was slowly varying with sharp local phase changes associated with blood flow near the bottom of the image and in several locations around the circumference of the brain.

Partial data sets were generated by setting the values for $u < -m$ equal to 0 in the full data sets. Each partial Fourier algorithm was tested on the clinical images with the filtered (low frequency), the generalized series (GS) and the 2D polynomial estimate. The low frequency phase estimate (2) uses as a phase estimate the image generated by zero padding the center portion of the data $-m \leq u < m$ to $-N/2 \leq u < N/2$ and reconstructing using the standard Fourier technique. By contrast, the generalized series (9) attempts to model all the known frequency information using a separable function where one component contains only image amplitude terms (based on an edge enhanced magnitude image) and the other only phase information. Further details may be found in the review by Liang *et al.* (8).

MacFall *et al.* (16) have attempted to generate a phase estimate using a 1D polynomial. This work was extended first by Berstein and Perman (12) to low order polynomials in both data directions and then by McGibney *et al.* (10, 11) to a true 2D polynomial fit. A major advantage of

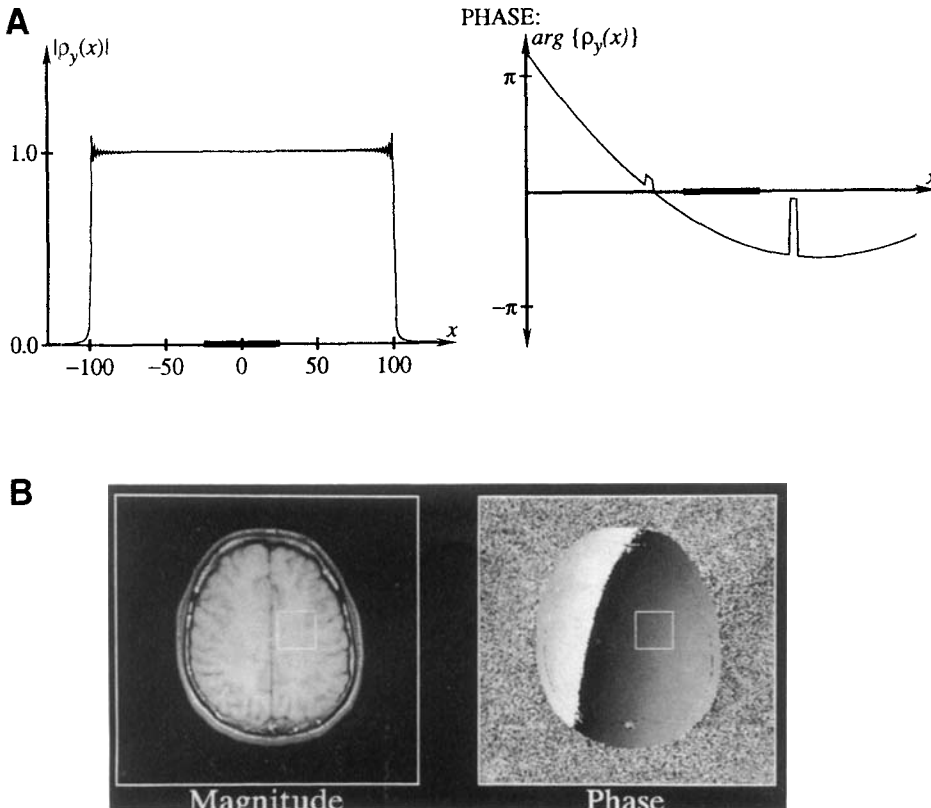


FIG. 6. (A) Artificial box data with several discontinuities superimposed on a general quadratic phase shift. The heavy line indicates the area used for local error determination. (B) Full clinical image with several location of large (rapid) phase changes. The box indicates the area used for local error determination.

the polynomial estimators is that they give “smooth” phase estimates. This generates a narrow band-width phase estimator, which should reduce the edge effects associated with the phase correction operator. For the images used in this analysis the full width at tenth maximum of the phase estimators for the 2D polynomial, filtered and GS algorithms was 5, 17, and 217 pixels, respectively. For a gradient echo image, the Margosian phase estimate would have the lowest bandwidth as there currently is not a suitable smooth phase estimator for this class of image (10). A quantitative comparison of the phase estimators used with both spin and gradient echo images is to be the subject of a future paper.

A quantitative analysis was made to evaluate the effectiveness of the partial Fourier algorithms. Difference images, determined by subtracting the magnitude of the partial Fourier image, $\rho_{partial}(x, y)$, from the magnitude of the full Fourier reconstruction, $\rho_{full}(x, y)$, were evaluated. All tests were done using partial Fourier data sets with $m = 16$. The short length of the symmetrically sampled data will tend to emphasize any reconstruction problems. To further emphasize the phase effects, both data sets were deliberately offset by 2 pixels to ensure that the data was asymmetrically positioned relative to the expected “center.” The power error measure,

$$error = \frac{\sum_{(x,y) \in R} (|\rho_{partial}| - |\rho_{full}|)^2}{\sum_{(x,y) \in R} (|\rho_{full}|)^2} \cdot 100\% \quad [5]$$

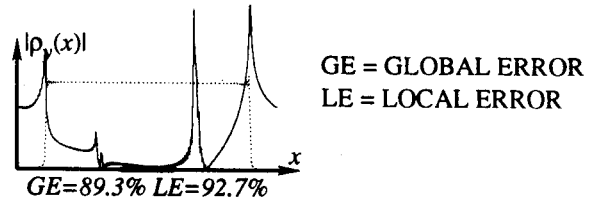
indicates the relative size of the difference image to the full Fourier image. It was applied over regions, R, that covered the full image and a small region. The full image measure is a global estimate of the overall quality of the phase fit, including regions of rapid phase change where phase estimation can be difficult. The second small region evaluation measures the quality of the reconstruction away from these difficult regions. Any increased error in the local error measure indicates that image distortion has been introduced by the poor reconstruction of other areas.

Figure 7 provides a comparison of the partial Fourier reconstruction of the artificial box image when used with the various phase estimation algorithms. The corresponding quantitative error measures are given below the figures. The degree to which inaccuracies in one image portion affect other image areas should be examined. The local error area is indicated by the thick line in the figures. Figure 8 show the difference images together with the quantitative measures for the full image data. The local area chosen for quantitative evaluation is indicated by a small box in the full image (Fig. 6B).

The conjugate synthesis results are included for completeness. All test images indicated that when any phase terms are present, the basic assumption of this method is invalid and unacceptable reconstruction occurs.

The Margosian and homodyne detection reconstructions are equivalent except that they display a magnitude and a real component image respectively, which should have no effect on the measures for the high SNR images analyzed. When any phase term is present, the systematic errors caused by the phase convolution distortions dis-

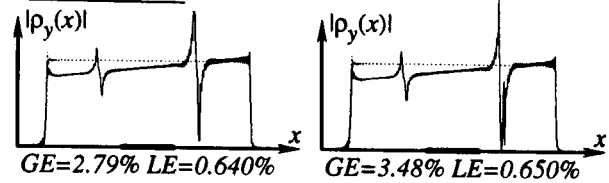
CONJUGATE SYNTHESIS



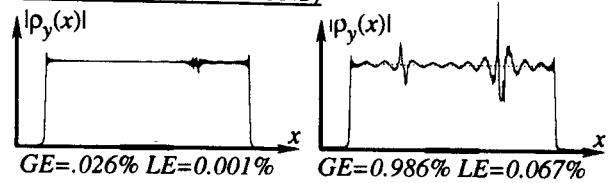
EXACT ESTIMATE

INCORRECT ESTIMATE

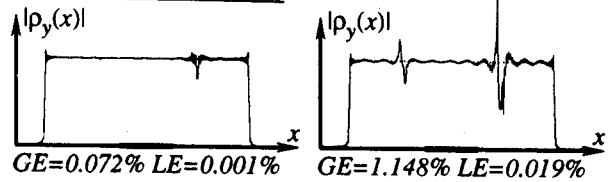
MARGOSIAN



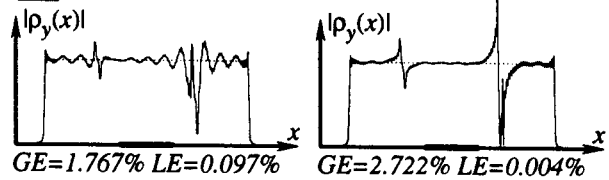
CUPPEN (4 ITERATIONS)



POCS (4 ITERATIONS)



FIR



MoFIR

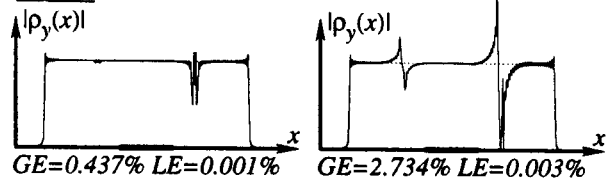


FIG. 7. Artificial box data reconstructed using the different partial Fourier reconstruction algorithms in conjunction with various phase estimation algorithms. The global and local error values are indicated.

cussed earlier can be seen in all test images as errors in the DC and very low frequency image components. However, these errors are greatly reduced from the complex

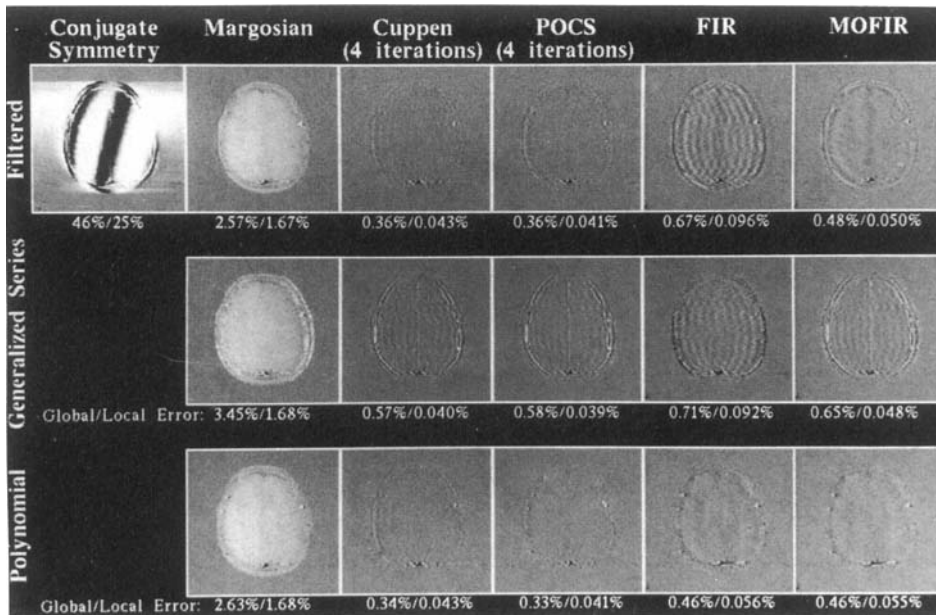


FIG. 8. Difference images for the clinical data reconstructed using partial Fourier reconstruction methods in conjunction with various phase estimation techniques. Global and local error values are indicated.

synthesis approach for only a small increase in computation time.

Given the exact phase terms, both the Cuppens and POCS iterative approaches quickly move to a line image that is equivalent to that of the full Fourier reconstruction. In practice, the phase estimate will not be exact and the procedures have a tendency to become unstable in this situation if iterated too often. Given an inaccurate phase estimate (quadratic terms only), the Cuppen algorithm had large amplitude distortions in the regions of local rapid phase change which spread as low frequency oscillations into areas where the phase estimate had been correct. The rippling occurs because of the mismatch of the positive and negative data sets where they meet in the frequency domain; producing Gibbs' ringing artifacts in the image domain. This ringing is particularly evident in the full image when the phase estimate is generated from the generalized series algorithm as this approach is itself susceptible to ringing artifacts (10). The POCS convergence is slower than for the Cuppen's algorithm because of the averaging action. However, the local phase error effects do not spread as far through the image because of the smoothing action of the averaging and the use of a merging filter.

Because the high frequency bandwidth of the exact phase estimate invalidates its basic assumptions, the *FIR* method performs poorly on the artificial box data. With the lower bandwidth of the smoothed phase estimate, it provides a reconstruction on both the line and clinical data similar to the Cuppen or POCS algorithms, with artifacts near the rapid phase changes. Unlike Cuppen and POCS reconstructions, these distortions are strictly localized to the area where the phase has been incorrectly determined (sharp changes). This localizing effect is also seen when the *FIR* is used on the clinical image with filtered and generalized series phase estimates, despite their larger bandwidth.

The *MoFIR* reconstruction approach was designed to work with both the low bandwidth 2D polynomial and

higher bandwidth filtered and generalized series phase estimates. This allows its use with both spin and gradient echo images, unlike the direct *FIR* approach. Errors from an inaccurate phase estimate are again localized, avoiding the systematic distortions found in the Margosian/homodyne detection reconstructions.

An estimate of the calculation time required for the algorithms was obtained by implementing the algorithm on a TAAC application's accelerator connected to a SUN 3/160 workstation and does not include system overhead such as image movement. The results are given in Table 1. The times for phase estimation plus partial Fourier reconstruction range over several orders of magnitude. The times for POCS reconstruction is for the faster algorithm suggested by McGibney (10). The actual times for the Cuppen and POCS algorithms depends on the number of iterations required, which is image-dependent.

Despite the fact that the *FIR* reconstruction used a small bandwidth filter during the direct convolution, it

Table 1
Comparison of the Times of the Partial Fourier Reconstruction Algorithms Both Individually and in Conjunction with the Phase Estimation Algorithms

	Partial Fourier only (s)	Partial Fourier plus filtered estimate (s)	Partial Fourier plus generalized series estimate (s)	Partial Fourier plus polynomial estimate (s)
Conjugate-symmetry	2.4	7.1	464	7.1
Margosian-homodyne	2.9	7.6	464	7.6
Cuppen (4 iterations)	12.5	17.2	474	17.2
POCS (4 iterations)	14.6	19.3	476	19.3
<i>FIR</i> (direct)	9.6	14.3	471	14.3
<i>FIR</i> (circular)	5.3	10.0	467	10.0
<i>MoFIR</i> (circular)	5.3	10.0	467	10.0

was still considerably slower than the *MoFIR* reconstruction which required a number of additional transforms between the frequency and time domains. This is a consequence of the $2pN$ and $N\log_2 N$ time relationship between the direct and circular convolution methods. In retrospect, the *FIR* reconstruction, despite its shorter filter length, could also have been determined this way. The current implementation of the Cuppen and POCS algorithms via the computationally efficient circular convolution must be balanced against the fact that the circular convolution mixes the high positive and negative data frequencies. Direct convolution can allow better control of the edge effects. By contrast, there is no difference in the *FIR* and *MoFIR* algorithms implemented by either approach. This is because there are not yet any negative frequency data components when the phase correction convolution is applied.

CONCLUSIONS

Five existing methods of partial Fourier imaging (conjugate symmetry, Margosian, homodyne detection, Cuppen, and POCS) were analyzed using equivalent frequency domain operations to determine how they introduced the missing data and what their weaknesses were. The analysis was used to suggest two new partial reconstruction techniques (*FIR* and *MoFIR*) in an attempt to obtain the best features of the other algorithms but in a faster implementation.

Global and local quantitative measures of the algorithms was made using an artificial 1D image and a 2D clinical images. Similar distortion effects and systematic errors were seen for the algorithms whether reconstructing artificial or clinical data with the conjugate symmetry, Margosian and homodyne approaches giving the worst results.

The Cuppen and POCS algorithms converged to the exact image (given enough iterations) if a true phase estimate was provided. However, if the phase estimate was not exact, both algorithms produced major non-localized artifacts. However, their global performance was better than the other algorithms.

The *FIR* and *MoFIR* methods are fast non-iterative algorithms implemented using an approach that allowed for the correction of edge effects associated with the phase correction operation. When the phase estimate was not exact, artifacts were produced as with the other reconstruction approaches. Unlike the other reconstructions, these inaccuracies were confined to the region of the error and did not produce significant ringing in the correctly phase estimated areas. The *MoFIR* algorithm was the more stable in the presence of high frequency phase components, making it applicable for both spin and gradient echo reconstructions.

All the algorithms performed the best with a low bandwidth phase estimator. Through frequency domain analysis of the partial Fourier reconstruction algorithms we have shown the importance of properly accounting for the edge effects associated with the phase correction techniques used in existing partial Fourier algorithms. These edge effects can be minimized when only small

values of the partial data width m are available by using a low bandwidth phase estimator and a narrow merging filter. In particular, the merging filter must be applied after the phase correction so that the merging filter characteristics are not distorted, and to ensure that the phase correction edge effects are removed. When only high bandwidth phase estimators are available, as in a gradient echo image, a larger value of m is required for optimal reconstruction. After phase correction, a sharp transition merging filter is used in the *MoFIR* algorithm to remove (reduce) the data made invalid by the phase correction convolution operation, and then the data is reflected and reconstructed.

However full removal of the edge effects can only be achieved by reconstructing using the undistorted data between $[-m + p \leq u < N/2 - 1 - 2p]$. This implies some technique, such as modeling (8, 17), to implicitly or explicitly extrapolate the data beyond $u = N/2 - 1 - 2p$ to avoid the convolution distortion associated with smearing the high positive and negative frequencies of the partial data set. In addition, since the phase estimator bandwidth may be greater than the partial data width, it will also be necessary to generate the data for $u \leq -m + 2p$. After these extrapolations, the partial Fourier reconstruction can be completed. A number of papers (10, 18, 19) have reported early results from the combination of modeling and partial Fourier reconstruction, although those algorithms were not implemented with the intention of removing the phase correction distortions. The quantitative evaluation of the joint technique is to be the subject of a future paper. The evaluation is difficult as it is necessary to distinguish between the effects of modeling on both the full Fourier and partial Fourier reconstructions and the correction of the phase estimation edge effects.

ACKNOWLEDGMENT

The authors wish to thank the University of Calgary and the Natural Sciences and Engineering Research Council (NSERC) of Canada for scholarship and operating funds. The clinical image was provided by Dr. Fernando Boada (Case Western Reserve University, Cleveland, Ohio).

REFERENCES

1. D. A. Feinberg, J. D. Hale, J. C. Watts, L. Kaufman, A. Mark, *Radiology* **161**, 527 (1986).
2. P. Margosian, in "Proceedings, 4th SMRM Conference," 1024 (1985).
3. P. Margosian, F. Schmitt, D. E. Purdy, *Health Care Instrum.* **1**, 195 (1986).
4. D. C. Nolls, D. G. Nishimura, A. Macovski, *IEEE Trans. Med. Imag.* **MI-10(2)**, 154 (1991).
5. J. Cuppen, A. van Est, *Magn. Reson. Imaging.* **5**, 526 (1987).
6. E. D. Lindskog, E. M. Haacke, J. D. Mitchel, Z. P. Liang, in "Proceedings, 8th SMRM Conference, 1989," p. 363.
7. E. M. Haacke, E. D. Lindskog, W. Lin, *J. Magn. Reson.* **92**, 126 (1991).
8. Z. P. Liang, F. E. Boada, R. T. Constable, E. M. Haacke, P. C. Lauterbur, M. R. Smith, *Rev. Magn. Reson. Med.* **4(2)**, 67 (1992).
9. Z. P. Liang, in "Proceedings, 9th SMRM Conference, 1990," p. 552.

10. G. McGibney, "Phase Sensitive Reconstruction of MR Images," M. Sc. thesis, Electrical and Computer Engineering, University of Calgary, Canada (1991).
11. G. McGibney, M. R. Smith, S. T. Nichols, in "Proceedings, 9th SMRM Conference, 1990," p. 563.
12. M. A. Bernstein, W. H. Perman, in "Proceedings, 6th SMRM Conference, 1987," p. 801.
13. M. A. Bernstein, D. M. Thomasson, W. H. Perman, *Med. Phys.* **16**(5), 813 (1989).
14. J. Hua, G. C. Hurst, *J. Magn. Res. Imaging* **2**, 347 (1992).
15. E. D. Lindskog, "Partial Fourier Imaging," M.Sc. thesis, Department of Electrical Engineering and Applied Physics, Case Western Reserve University, (1989).
16. J. R. MacFall, N. J. Pelc, R. M. Vavrek, *Magn. Res. Imaging* **6**, 143 (1988).
17. M. Smith, S. T. Nichols, R. Constable, R. M. Henkelman, *Magn. Reson. Med.* **19**, 1 (1991).
18. M. R. Smith, W. Saar, S. T. Nichols, in "Proceedings, 5th SMRM Conference, 1986," p. 81.
19. J. M. Goldfarb, E. M. Haacke, F. E. Boada, W. Lin, in "Proceedings, 10th SMRM Conference, 1991," p. 1226.